Satellite-Based Energy Balance for Mapping Evapotranspiration with Internalized Calibration (METRIC)—Model

Richard G. Allen[1]; Masahiro Tasumi[2]; and Ricardo Trezza[3]

Abstract: Mapping evapotranspiration at high resolution with internalized calibration (METRIC) is a satellite-based image-processing model for calculating evapotranspiration (ET) as a residual of the surface energy balance. METRIC uses as its foundation the pioneering SEBAL energy balance process developed in The Netherlands by Bastiaanssen, where the near-surface temperature gradients are an indexed function of radiometric surface temperature, thereby eliminating the need for absolutely accurate surface temperature and the need for air-temperature measurements. The surface energy balance is internally calibrated using ground-based reference ET to reduce computational biases inherent to remote sensing-based energy balance and to provide congruency with traditional methods for ET. Slope and aspect functions and temperature lapsing are used in applications in mountainous terrain. METRIC algorithms are designed for relatively routine application by trained engineers and other technical professionals who possess a familiarity with energy balance and basic radiation physics. The primary inputs for the model are short-wave and long-wave (thermal) images from a satellite (e.g., Landsat and MODIS), a digital elevation model and ground-based weather data measured within or near the area of interest. ET "maps" (i.e., images) via METRIC provide the means to quantify ET on a field-by-field basis in terms of both the rate and spatial distribution. METRIC has some significant advantages over many traditional applications of satellite-based energy balance in that its calibration is made using reference ET, rather than the evaporative fraction. The use of reference ET for the extrapolation of instantaneous ET from periods of 24 h and longer compensates for regional advection effects by not tying the evaporative fraction to net radiation, since ET can exceed daily net radiation in many arid or semi-arid locations. METRIC has some significant advantages over conventional methods of estimating ET from crop coefficient curves in that neither the crop development stages, nor the specific crop type need to be known with METRIC. In addition, energy balance can detect reduced ET caused by water shortage.

DOI: 10.1061/(ASCE)0733-9437(2007)133:4(380)

CE Database subject headings: Evapotranspiration; Energy balance; Netherlands; Temperature measurement; Water shortage; Satellites; Calibration; Metric system.

Introduction

Land surface evapotranspiration (ET) transfers large volumes of water from soil (evaporation) and vegetation (transpiration) to the atmosphere. Quantifying the consumption of water over large areas and within irrigated projects is important for water rights management, water resources planning, hydrologic water balances, and water regulation. The differences between the actual and potential ET at high spatial resolutions are of interest to agriculture, water resources, and even national security, as an indicator of crop water deficits. Spatial estimates of ET are essential components of general circulation and hydrologic models (Wigmosta et al. 1994; Betts et al. 1997) and ET is used to infer soil moisture, a valuable input to weather and flood forecast models. Sensible and latent heat fluxes can severely impact the performance of optical, infrared, and acoustic sensors used by the military. ET and soil moisture affect the operational mobility of military operations and detection of landmines and unexploded ordinance (Van Dam et al. 2005).

Traditionally, ET from agricultural fields has been estimated by multiplying a weather-based reference ET by a crop coefficient (K_c) determined according to the crop type and growth stage. However, there is typically some question as to whether actual vegetative and growing conditions compare with the conditions represented by the idealized K_c values, especially in water short areas. In addition, it is difficult to predict the correct crop growth stage dates for large populations of crops and fields. Satellite data are ideally suited for deriving spatially continuous fields of ET using energy balance techniques. Mapping evapotranspiration at high resolution with internalized calibration (METRIC) is a satellite-based image-processing tool for calculating ET as a residual of the energy balance at the Earth's surface. METRIC has, as its foundation, principles and techniques used by the important model SEBAL, an energy balance model developed in The Netherlands and applied worldwide by Bastiaanssen and his associates (1995, 1998a,b, 2000, 2005). The innovative component of

[1]Professor, Kimberly Research Center, Univ. of Idaho, Kimberly, ID 83341. E-mail: rallen@kimberly.uidaho.edu

[2]Associate Professor, Univ. of Miyazaki, 1-1, Gakuen Kibanadai-Nishi, Miyazaki 889-2192, Japan. E-mail: tasumi@cc.miyazaki-u.ac.jp

[3]Visiting Professor, Kimberly Research Center, Univ. of Idaho, Kimberly, ID 83341. E-mail: rtrezza@kimberly.uidaho.edu

Note. Discussion open until January 1, 2008. Separate discussions must be submitted for individual papers. To extend the closing date by one month, a written request must be filed with the ASCE Managing Editor. The manuscript for this paper was submitted for review and possible publication on November 16, 2005; approved on March 16, 2007. This paper is part of the ***Journal of Irrigation and Drainage Engineering***, Vol. 133, No. 4, August 1, 2007. ©ASCE, ISSN 0733-9437/2007/4-380–394/$25.00.

SEBAL is that the energy balance modeling uses a near-surface temperature gradient, dT, which is indexed to the radiometric surface temperature. This has eliminated the need for absolute surface temperature calibration, a major stumbling block in operational satellite ET. METRIC uses the SEBAL technique for estimating dT, thereby eliminating the need for an absolutely accurate aerodynamic surface temperature and the need for air-temperature measurements for estimating sensible heat flux at the surface.

METRIC departs from the SEBAL model in its use of weather-based reference ET to establish energy balance conditions at a "cold" pixel. This innovation makes the best use of existing technology in agricultural areas, and establishes a ground reference for the satellite-based actual ET estimate. It effectively serves as a "reality check" on actual ET estimates. In METRIC, the satellite-based energy balance is internally calibrated at two extreme conditions (dry and wet) using locally available weather data. The autocalibration is done for each image using an alfalfa-based reference ET (ET_r) computed from hourly weather data. The accuracy and dependability of the ET_r estimate has been established by lysimetric and other studies in which we have high confidence (ASCE-EWRI 2005). The internal calibration of the sensible heat computation within SEBAL and METRIC, and the use of the indexed temperature gradient, eliminate the need for refined atmospheric correction of the surface temperature (T_s) and reflectance (albedo) measurements using radiative transfer models (Tasumi et al. 2005b). The internal calibration also reduces impacts of biases in the estimation of aerodynamic stability correction and surface roughness, as described later. In this paper, we present the theoretical basis and operational algorithms of the METRIC model. A companion paper by Allen et al. (2007) describes applications in Idaho where METRIC has been used to monitor water-right compliance and aquifer depletion, as a tool for water resource planning, and in hydrologic models in the Rio Grande Valley of New Mexico, where METRIC has been used to map ET from agricultural and riparian vegetation along a narrow river corridor, and in the Imperial Valley of California, where METRIC ET maps have been used to assess irrigation adequacy and salinity management.

METRIC is designed to produce high-quality accurate maps of ET for focused regions smaller than a few hundred kilometers in scale and at high resolution. This contrasts with some remote sensing models that are more generally based and are designed for routine application over large regions (for example, over subcontinents), such as the atmosphere-land exchange inverse (ALEXI) model (Anderson et al. 2004), the feedback method of Granger (1989, 2000), and SEBAL as applied with AVHRR and MODIS imagery (Bastiaanssen et al. 2005). The narrowed focus of METRIC is intended to provide relatively more accurate estimates of ET at higher resolution (~30 m) as compared with more general models, and to account for impacts of regional advection. The narrowed focus does come at a cost; however, in the requirement for trained experts who possess a strong background in energy balance and radiation physics and an adequate knowledge of vegetation characteristics, as well as the requirement for high-quality hourly (or shorter) weather data. METRIC has some significant advantages over the traditional applications of satellite-based energy balance (Bastiaanssen et al. 1998a; Bastiaanssen 2000) in that its calibration is made using reference ET, rather than the evaporative fraction. The use of reference ET for the extrapolation of instantaneous ET from periods of 24 h and longer compensates for regional advection effects by not tying the evaporative fraction to net radiation, since ET can exceed daily net radiation in many arid or semi-arid locations. METRIC has some significant advantages over conventional methods of estimating ET from crop coefficient curves in that neither crop development stages nor the specific crop type need to be known with METRIC. In addition, energy balance can detect reduced ET caused by water shortage.

Theoretical Basis

The theoretical and computational basis of SEBAL is described in Bastiaanssen et al. (1998a), Bastiaanssen (2000), and Bastiaanssen et al. (2005). Although satellites routinely measure surface reflectance and some measure surface temperature, none measure near-surface vapor content. Therefore, ET is generally determined from satellite imagery by applying an energy balance at the surface, where energy consumed by the ET process is calculated as a residual of the surface energy equation

$$\mathrm{LE} = R_n - G - H \tag{1}$$

where LE=latent energy consumed by ET; R_n=net radiation (sum of all incoming and outgoing short-wave and long-wave radiation at the surface); G=sensible heat flux conducted into the ground; and H=sensible heat flux convected to the air. The parameters in Eq. (1) are generally expressed in W m^{-2}. One utility of using energy balance is that actual ET rather than potential ET (based on amount of vegetation) is computed so that reductions in ET caused by a shortage of soil moisture are captured. A primary disadvantage of the energy balance approach is that the computation of LE is only as accurate as the summed estimates for R_n, G, and H. METRIC attempts to overcome this disadvantage by focusing internal calibration not on LE but on H to absorb all intermediate estimation errors and biases.

In METRIC, R_n is computed from the satellite-measured narrow-band reflectance and surface temperature; G is estimated from R_n, surface temperature, and vegetation indices; and H is estimated from surface temperature ranges, surface roughness, and wind speed using buoyancy corrections. The algorithms used in METRIC for R_n and G stem from those used in early SEBAL applications by Bastiaanssen et al. (1998a). However, albedo in METRIC was updated following Tasumi et al. (2007) to improve accuracy over a wide range of surface conditions.

Net Radiation

Actual net radiation flux at the surface (R_n) represents the radiant energy at the surface that is partitioned into H, G, and LE. R_n is computed by subtracting all outgoing radiant fluxes from all incoming radiant fluxes and includes solar and thermal radiation

$$R_n = R_{S\downarrow} - \alpha R_{S\downarrow} + R_{L\downarrow} - R_{L\uparrow} - (1 - \varepsilon_o) R_{L\downarrow} \tag{2}$$

where $R_{S\downarrow}$=incoming short-wave radiation (W m^{-2}); α=surface albedo (dimensionless); $R_{L\downarrow}$=incoming long-wave radiation (W m^2); $R_{L\uparrow}$=outgoing long-wave radiation (W m^2); and ε_o=broad-band surface thermal emissivity (dimensionless). The $(1-\varepsilon_o)R_{L\downarrow}$ term represents the fraction of incoming long-wave radiation reflected from the surface.

Incoming Solar Radiation

Incoming broad-band short-wave radiation, as direct and diffuse at the Earth's surface (W m^2), represents the principal energy source for ET. For images having little slope, $R_{s\downarrow}$ can be calculated for the image time as a constant over the image, provided

the image area is smaller than about 25,000 km^2 (i.e., one Landsat image), and assuming clear sky conditions, since clear sky is a prerequisite to a useable satellite image

$$R_{s\downarrow} = \frac{G_{sc} \cos \theta_{rel} \tau_{sw}}{d^2} \quad (3)$$

where G_{sc}=solar constant (1367 W m^{-2}); θ_{rel}=solar incidence angle; d^2=square of the relative Earth–Sun distance; and τ_{sw}=broad-band atmospheric transmissivity. For mountainous scenes, $R_{s\downarrow}$ must be computed for each pixel of the scene using Eq. (7) for θ_{rel}. Calculated $R_{s\downarrow}$ for clear sky conditions is considered to have the same or better accuracy as measured $R_{s\downarrow}$ from an automated weather station (Allen 1996; ASCE-EWRI 2005). τ_{sw} is calculated using a general function from ASCE-EWRI (2005)

$$\tau_{sw} = 0.35 + 0.627 \exp\left[\frac{-0.00146P}{K_t \cos \theta_{hor}} - 0.075\left(\frac{W}{\cos \theta_{hor}}\right)^{0.4}\right] \quad (4)$$

where P=atmospheric pressure (kPa); W=water in the atmosphere (mm); and θ_{hor}=solar zenith angle over a horizontal surface [from Eq. (8)]. K_t=unitless turbidity coefficient $0 < K_t \leq 1.0$, where K_t=1.0 for clean air and K_t=0.5 for extremely turbid, dusty, or polluted air (Allen 1996; Allen et al. 1998). $P/(\cos \theta_{hor})$=surrogate for atmospheric mass and optical path length. The exponential function follows Beer's law for radiation extinction. Eq. (4) is valid for θ less than about 1.3 radians. P, kPa, is calculated by ASCE-EWRI (2005) as

$$P = 101.3\left(\frac{293 - 0.0065z}{293}\right)^{5.26} \quad (5)$$

where 293=standard air temperature (K), as used by EWRI in their ET standardization, and z=elevation above sea level (m). W is calculated using measured or estimated near-surface vapor pressure from a representative weather station, according to the equation by Garrison and Adler (1990)

$$W = 0.14 e_a P_{air} + 2.1 \quad (6)$$

where e_a=near-surface vapor pressure (kPa), and W is in mm.

The solar incidence angle is the angle between the solar beam and a vertical line perpendicular to the land surface. For horizontal flat surfaces, θ_{rel} is simply equivalent to solar zenith angle (i.e., $\pi/2$ minus the solar elevation angle). However, for sloping surfaces, θ_{rel} in Eq. (3) must be calculated pixel by pixel, using the surface slope and aspect information derived from a digital elevation model and the following equation from Duffie and Beckman (1991)

$$\begin{aligned}\cos \theta_{rel} = {} & \sin(\delta)\sin(\phi)\cos(s) - \sin(\delta)\cos(\phi)\sin(s)\cos(\gamma) \\ & + \cos(\delta)\cos(\phi)\cos(s)\cos(\omega) \\ & + \cos(\delta)\sin(\phi)\sin(s)\cos(\gamma)\cos(\omega) \\ & + \cos(\delta)\sin(\gamma)\sin(s)\sin(\omega)\end{aligned} \quad (7)$$

where δ=declination of the Earth (positive in summer in the northern hemisphere); ϕ=latitude of the pixel (positive for the northern hemisphere and negative for the southern hemisphere); s=surface slope, where $s=0$ for horizontal and $s=\pi/2$ radians for vertical downward slope (s is always positive and represents the downward slope in any direction); γ=surface aspect angle, where $\gamma=0$ for slopes oriented due south, $\gamma=-\pi/2$ radians for slopes oriented due east, $\gamma=+\pi/2$ radians for slopes oriented due west, and $\gamma=\pm\pi$ radians for slopes oriented due north. Parameter ω is the hour angle, where $\omega=0$ at solar noon, ω is negative in morning, and ω is positive in afternoon. All trigonometric functions are in radians. For a "flat" application, where slope and aspect are ignored, Eq. (7) reduces to

$$\cos \theta_{hor} = \sin(\delta)\sin(\phi) + \cos(\delta)\cos(\phi)\cos(\omega) \quad (8)$$

which is the solar angle used in Eq. (4). Reprojection of the final ET determined for slopes to a horizontal equivalent can be done by dividing by the cosine of the slope.

Parameter d^2 is calculated as a function of the day of the year (DOY) using Duffie and Beckman (1991)

$$d^2 = \frac{1}{1 + 0.033 \cos(\text{DOY } 2\pi/365)} \quad (9)$$

where DOY=day of the year and (DOY$\times 2\pi/365$) is in radians. Equations for declination of the Earth and time corrections for calculating ω and solar time from local time are standard equations available from Duffie and Beckman (1980, 1991), Allen (1996), ASCE-EWRI (2005), and other sources.

Surface Albedo

Surface albedo, the ratio of reflected solar radiation to the incident solar (short-wave) radiation at the surface, represents the integrated reflectance across the short-wave spectrum (0.2 to 3.2 micrometers). Albedo is calculated by integrating reflectivities from representative satellite bands, for example, bands 1–5 and 7 of Landsat, bands 1–7 of MODIS, and bands 1–9 of ASTER. "At-satellite" or "top of atmosphere" reflectance ($\rho_{t,b}$) of a band (b) is a bidirectional (BD) reflectance calculated for each band from at-satellite directional radiance

$$\rho_{t,b} = \frac{\pi L_{t,b} d^2}{ESUN_b \cos \theta_{rel}} \quad (10)$$

where spectral radiance $L_{t,b}$=reflected energy measured in band b of the satellite (W m^{-2} ster^{-1} μm^{-1}), $ESUN_b$ is the mean solar exoatmospheric radiation over band b (W m^{-2} μm^{-1}); θ_{rel}=solar incidence angle (or solar zenith angle) relative to the normal to the land surface slope; and d=Earth–Sun distance in astronomical units. Values for $ESUN_b$ are presented in Chander and Markham (2003) for Landsat 4 and 5, in LPSO (2004) for Landsat 7, and in Tasumi et al. (2007) for MODIS satellites.

Eq. (10) produces BD reflectance at the satellite, whereas actual reflectance at the surface, $\rho_{s,b}$, is needed to calculate surface albedo, which is predominately directional hemispherical. In METRIC, we derive predominantly BD at-surface reflectance at satellite image time using calibrated atmospheric transmittance and path reflectance functions by Tasumi et al. (2007). This BD at-surface reflectance is similar to the predominately directional-hemispherical reflectance during midday. The functions by Tasumi et al. (2007) correct $\rho_{t,b}$ for scattering and absorption of incoming and reflected solar radiation from the surface based on a simplified atmospheric correction function that requires only point measurements or estimates of near-surface vapor pressure; e_a. The Tasumi function was designed for use in routine operational applications of the METRIC energy balance. Atmospheric correction can be done using more sophisticated models, such as MODTRAN (Berk et al. 1999) that account for the impacts of humidity, temperature, and aerosol profiles on scattering and absorption. However, these models generally require good background knowledge of the correction model and the software program, which is not common to irrigation engineering professionals, and some effort to apply. In METRIC, small biases in $\rho_{s,b}$

Table 1. Constants C_1 to C_5 in Eqs. (12) and (13), C_b in Eq. (14), and W_b in Eq. (15) for Use with Landsat Images (Adapted from Tasumi et al. 2007)

Coefficient	Band 1	Band 2	Band 3	Band 4	Band 5	Band 7
C_1	0.987	2.319	0.951	0.375	0.234	0.365
C_2	−0.00071	−0.00016	−0.00033	−0.00048	−0.00101	−0.00097
C_3	0.000036	0.000105	0.00028	0.005018	0.004336	0.004296
C_4	0.0880	0.0437	0.0875	0.1355	0.0560	0.0155
C_5	0.0789	−1.2697	0.1014	0.6621	0.7757	0.639
C_b	0.640	0.310	0.286	0.189	0.274	−0.186
W_b	0.254	0.149	0.147	0.311	0.103	0.036

resulting from the simplified correction procedure are corrected for during the internal calibration of sensible heat flux, as described later.

At-surface reflectance for band b, $\rho_{s,b}$, is estimated as

$$\rho_{s,b} = \frac{R_{\text{out},s,b}}{R_{\text{in},s,b}} = \frac{\rho_{t,b} - \rho_{a,b}}{\tau_{\text{in},b} \cdot \tau_{\text{out},b}} \tag{11}$$

where $R_{\text{in},s,b}$ and $R_{\text{out},s,b}$ (W m^{-2} μm^{-1})=at-surface hemispherical incoming and reflected radiances; $\tau_{\text{in},b}$=effective narrowband transmittance for incoming solar radiation; and $\tau_{\text{out},b}$=effective narrowband transmittance for shortwave radiation reflected from the surface. $\tau_{\text{in},b}$ and $\tau_{\text{out},b}$ account for attenuation of both beam and diffuse radiation. $\tau_{a,b}$ is an atmospheric path reflectance for band b that represents solar radiation backscattered by the atmosphere to the satellite. Parameters $\tau_{\text{in},b}$ and $\tau_{\text{out},b}$ are calculated using individually derived equations for each band of the satellite and $\rho_{a,b}$ was calibrated by Tasumi et al. (2007) for each band as a function of transmittance.

The transmittance functions for $\tau_{\text{in},b}$ and $\tau_{\text{out},b}$ by Tasumi et al. (2007) follow a common format similar to the broad-band (global) transmittance function of Majumdar et al. (1972) that was adapted by FAO and EWRI standardizations for calculating evapotranspiration (Allen et al. 1998; ASCE-EWRI 2005)

$$\tau_{\text{in},b} = C_1 \exp\left[\frac{C_2 P}{K_t \cos\theta_{\text{hor}}} - \frac{C_3 W + C_4}{\cos\theta_{\text{hor}}}\right] + C_5 \tag{12}$$

$$\tau_{\text{out},b} = C_1 \exp\left[\frac{C_2 P}{K_t \cos\eta} - \frac{C_3 W + C_4}{\cos\eta}\right] + C_5 \tag{13}$$

where C_1–C_5=fitted satellite-dependent constants, and the solar zenith angle θ_{hor} from Eq. (8) =the solar incident angle relative to the perpendicular from a horizontal flat surface (i.e., $\pi/2$ minus solar elevation angle), where the horizontal surface orientation is used even for application in mountainous terrain in order to properly estimate relative atmospheric thickness. Parameter η in Eq. (13) =the sensor (satellite) view angle relative to the perpendicular from a flat horizontal surface, which is zero for a nadir view and $\pi/2$ radians for a horizontal view angle. Landsat has essentially a nadir view angle, and thus cos η is 1. MODIS image sensor angles vary each day, occasionally exceeding $\pi/4$ radians (50°) and therefore η changes by image and/or pixel. The sensor-dependent constants C_1–C_5 in Eqs. (12) and (13) and the atmospheric path reflectance of each band, $\rho_{a,b}$ in Eq. (11) were calibrated using radiative transfer models, and are listed in Tables 1 and 2 for use with Landsat and MODIS satellites.

The value for $\tau_{\text{in},b}$ can vary from that for $\tau_{\text{out},b}$ due to impacts of backscattered diffuse radiation originating from radiation from the reflected surface that is contained in $\tau_{\text{in},b}$ but not in $\tau_{\text{out},b}$. However, $\tau_{\text{out},b}$ was found to be sufficiently well approximated using the same coefficients as for incoming transmittance, but with an equivalent atmospheric path length calculated for the angle between the land surface and sensor (i.e., satellite). Mean biases caused by small differences between $\tau_{\text{in},b}$ and $\tau_{\text{out},b}$ were incorporated into the $\rho_{a,b}$ term of Eq. (11) during calibration.

Path reflectance is some proportion of the amount of one-way scattered and absorbed radiation as represented by $1-\tau_{\text{in},b}$

$$\rho_{a,b} = C_b(1 - \tau_{\text{in},b}) \tag{14}$$

where C_b=determined scaling ratio for band "b" with values reported in Tables 1 and 2 for Landsat and MODIS satellites.

Broadband Surface Albedo from Integration of Narrowband At-Surface Reflectances

Broad-band surface albedo is calculated by integrating band reflectances within the short-wave spectrum using a weighting function

$$\alpha_s = \sum_{b=1}^{n} [\rho_{s,b} w_b] \tag{15}$$

where w_b=weighting coefficient (Tables 1 and 2) representing the fraction of at-surface solar radiation occurring within the spectral range represented by a specific band, and n is the number of satellite bands integrated. Tasumi et al. (2007) found good agreement between Eqs. (10)–(15) and albedo as determined by MODIS satellite. The METRIC albedo method is recommended for image portions with sensor view angles of 20° or

Table 2. Constants C_1 to C_5 in Eqs. (12) and (13), C_b in Eq. (14), and W_b in Eq. (15) for Use with MODIS Images (Adapted from Tasumi et al. 2007)

Coefficient	Band 1	Band 2	Band 3	Band 4	Band 5	Band 6	Band 7
C_1	1.102	0.451	0.996	1.944	0.318	0.216	0.275
C_2	−0.00023	−0.00023	−0.00071	−0.00016	−0.00022	−0.00050	−0.00031
C_3	0.000290	0.000550	0.000036	0.000105	0.000640	0.000800	0.004296
C_4	0.0875	0.0900	0.0880	0.0540	0.0760	0.0940	0.0155
C_5	−0.0471	0.5875	0.0678	−0.8870	0.7100	0.8006	0.7282
C_b	0.262	0.397	0.679	0.343	0.680	0.639	−0.464
W_b	0.215	0.215	0.242	0.129	0.101	0.062	0.036

less. All portions of Landsat images have a near-nadir sensor view angle.

Outgoing Long-Wave Radiation

Outgoing long-wave radiation, $R_{L\uparrow}$, emitted from the surface is driven by surface temperature and surface emissivity. $R_{L\uparrow}$ is computed using the Stefan–Boltzmann equation

$$R_{L\uparrow} = \varepsilon_0 \sigma T_s^4 \tag{16}$$

where ε_0=broad-band surface emissivity (dimensionless); σ=Stefan–Boltzmann constant (5.67×10^{-8} W m^{-2} K^{-4}), and T_s=surface temperature (K). Surface emissivity is computed using an empirical equation by Tasumi (2003) based on soil and vegetative thermal spectral emissivities housed in the MODIS UCSB Emissivity Library (2004)

$$\varepsilon_0 = 0.95 + 0.01 \text{ LAI} \quad \text{for LAI} \leq 3 \tag{17}$$

and ε_0=0.98 when LAI>3, where LAI (m^2 m^{-2})=leaf area index; the ratio of the total leaf area for the surface (one side of leaves) per unit of ground area. LAI is an indicator of biomass and canopy resistance to vapor flux, and is computed using an empirical equation stemming from Bastiaanssen (1998a)

$$\text{LAI} = -\frac{\ln[(0.69 - \text{SAVI}_{ID})/0.59]}{0.91} \tag{18}$$

where, for Landsat images, SAVI 6 is based on top of atmosphere reflectance of bands 3 and 4

$$\text{SAVI} = \frac{(1+L)(\rho_{t,4} - \rho_{t,3})}{L + (\rho_{t,4} + \rho_{t,3})} \tag{19}$$

where SAVI=soil adjusted vegetation index (Huete 1988), and L=constant, often set to L=0.5. For METRIC applications in the western U.S., we use L=0.1, based on studies by Tasumi (2003) to minimize soil background biases, to create SAVI$_{ID}$. Eq. (18) produces a maximum value for LAI of 6.0, corresponding to SAVI$_{ID}$=0.69. Beyond SAVI$_{ID}$=0.69, the value for LAI "saturates" and does not change significantly. In METRIC, LAI is limited to 6.0 when SAVI$_{ID}$>0.687 and LAI=0 when SAVI$_{ID}$ <0.1. The accuracy of LAI estimation depends on site and soil characteristics and crop types (Bastiaanssen 1998a). Thus, Eqs. (18) and (19) may require local or regional calibration. However, the impact of error in LAI on the METRIC energy balance computation is small.

Surface temperature (T_s) is computed for Landsat images using a modified Plank equation following Markham and Barker (1986) with atmospheric and surface emissivity correction:

$$T_s = \frac{K_2}{\ln[(\varepsilon_{\text{NB}} K_1 / R_c) + 1]} \tag{20}$$

where ε_{NB}=narrow band emissivity corresponding to the satellite thermal sensor wave length band. R_c=corrected thermal radiance from the surface using spectral radiance $L_{t,6}$ from band 6 of Landsat, which is the thermal band. The K_1 and K_2 constants equal (K_1=607.8 and K_2=1261 W m^{-2} sr^{-1} μm^{-1} for Landsat 5 and K_1=666.1 and K_2=1283 W m^{-2} sr^{-1} μm^{-1} for Landsat 7).

R_c is calculated following Wukelic et al. (1989) as:

$$R_c = \frac{L_{t,6} - R_p}{\tau_{\text{NB}}} - (1 - \varepsilon_{\text{NB}}) R_{\text{sky}} \tag{21}$$

where $L_{t,6}$=spectral radiance of Landsat band 6 (W m^{-2} sr^{-1} μm^{-1}); R_p=path radiance in the 10.4–12.5 μm band (W m^{-2} sr^{-1} μm^{-1}); R_{sky}=narrow band downward thermal radiation from a clear sky (W m^{-2} sr^{-1} μm^{-1}); and τ_{NB}=narrow band transmissivity of air (10.4–12.5 μm range). Units for R_c are W m^{-2} sr^{-1} μm^{-1}.

Values for R_p and τ_{NB} require the use of an atmospheric radiation transfer simulation model, such as MODTRAN. In the absence of an atmospheric correction model, corrections in the calculation of R_c are ignored by setting R_p=0, τ_{NB}=1, and R_{sky}=0, and introduced biases are accounted for in the determination of the dT function. In METRIC applications in Idaho, values for R_p, τ_{NB}, and R_{sky} were determined from applications of MODTRAN for each image date. Similarity among values for R_p, τ_{NB}, and R_{sky} over a range of image dates during Spring, Summer, and Autumn indicated that mean values of R_p=0.91 W m^{-2} sr^{-1} μm^{-1}, τ_{NB}=0.866, and R_{sky}=1.32 W m^{-2} sr^{-1} μm^{-1} would produce more accurate and consistent values for R_c, in the absence of specific MODTRAN runs, than use of values R_p=0, τ_{NB}=1, and R_{sky}=0. The use of these default values for R_p, τ_{NB}, and R_{sky} provides general atmospheric correction for clear sky atmospheric conditions typical of the semiarid Idaho climate. Uncorrected R_c (R_p=0, τ_{NB}=1, and R_{sky}=0) tends to have good accuracy in the range of $260 < T_s < 285$ K, and tends to underestimate T_s by ~3–4 K at T_s around 315 K. However, the bias is relatively linear with T_s and is therefore generally compensated for during the creation of the dT function (Allen et al. 2005).

Narrow band transmissivity, ε_{NB}, representing the surface emissivity within the band range of the satellite thermal sensor, is estimated from Tasumi (2003) as

$$\varepsilon_{\text{NB}} = 0.97 + 0.0033 \text{ LAI}, \quad \text{for LAI} \leq 3 \tag{22}$$

and ε_{NB}=0.98 and ε_0=0.98 when LAI>3. Eq. (22) is applied when the normalized difference vegetation index (NDVI)>0, indicating soil or vegetation. NDVI≤0 indicates water or snow, where ε_{NB} and ε_o are estimated as 0.985.

The NDVI is the ratio of the differences in reflectivities for the near-infrared band and the red band to their sum. In case of Landsat, the corresponding bands are bands 4 and 3

$$\text{NDVI} = \frac{(\rho_{t,4} - \rho_{t,3})}{(\rho_{t,4} + \rho_{t,3})} \tag{23}$$

Incoming Long-Wave Radiation ($R_{L\downarrow}$)

Incoming long-wave radiation is the downward thermal radiation flux originating from the atmosphere (W m^{-2}) and is traditionally computed using the Stefan–Boltzmann equation

$$R_{L\downarrow} = \varepsilon_a \sigma T_a^4 \tag{24}$$

where ε_a=effective atmospheric emissivity (dimensionless), and T_a=near-surface air temperature (K). An empirical equation for ε_a by Bastiaanssen (1995) is applied by coefficients developed by Allen et al. (2000) and data collected over alfalfa in Idaho

$$\varepsilon_a = 0.85(-\ln \tau_{\text{sw}})^{0.09} \tag{25}$$

where τ_{sw}=broad-band atmospheric transmissivity for shortwave radiation calculated from Eq. (4). The original coefficients by Bastiaanssen (1995), derived for western Egypt, were $\varepsilon_a = 1.08(-\ln \tau_{\text{sw}})^{0.265}$. The T_a parameter in Eq. (24) is intended to be indexable to effective (radiometric) atmospheric temperature. In most applications of METRIC, the surface temperature (T_s) of each image pixel has been used as a surrogate for T_a in Eq. (24), which suggests that incoming long-wave varies across an image in proportion to the underlying surface temperature. In other applications, we have used a single value for T_a in Eq. (24) repre-

sented by T_s of the "cold" pixel, defined later. This is done to represent atmospheric conditions that are relatively homogeneous within a region. In mountainous terrain, T_a in Eq. (24)—when set equal to a fixed value for an image—is adjusted for lapse effects to simulate the net cooling of temperature aloft with elevation.

Soil Heat Flux (G)

Soil heat flux is the rate of heat storage in the soil and vegetation due to conduction. General METRIC applications compute G as a ratio G/R_n using an empirical equation by Bastiaanssen (2000) representing values near midday

$$\frac{G}{R_n} = (T_s - 273.15)(0.0038 + 0.0074\alpha)(1 - 0.98\ \mathrm{NDVI}^4) \tag{26}$$

where T_s=surface temperature (K), and α=surface albedo. G is then calculated by multiplying G/R_n by R_n. An alternative that has also been applied in METRIC was developed by Tasumi (2003) using soil heat flux data collected by Wright (1982). USDA-ARS for irrigated crops near Kimberly, Idaho

$$\frac{G}{R_n} = 0.05 + 0.18e^{-0.521\ \mathrm{LAI}} \quad (\mathrm{LAI} \geqslant 0.5) \tag{27a}$$

$$\frac{G}{R_n} = 1.80(T_s - 273.15)/R_n + 0.084 \quad (\mathrm{LAI} < 0.5) \tag{27b}$$

Eq. (27) has been used with applications in Idaho, California, and New Mexico. Both Eqs. (26) and (27) predict measured G relatively accurately for irrigated crops near Kimberly, Idaho (Tasumi 2003), and represent G/R_n for general agricultural soils that have been tilled within the last few hundred days; thus, they do not exhibit a large amount of cracking or delaminated crust. Eq. (26) suggests that G/R_n increases with increasing albedo (indicative of bare soils that often have high reflection) and decreases with increasing vegetation (due to shading by the canopy). Eq. (27a) suggests that G/R_n decreases with increasing leaf area, for the same reason, and Eq. (27b) suggests that for bare soil G increases in proportion to surface temperature. During some applications with METRIC to desert soils where near-surface thermal conductivities may be smaller than for tilled soils due to cracks, delaminated crust, lack of structure, or very low soil–water content, the G/R_n from Eq. (27b) is limited and even reduced for T_s more than T_s of the hot pixel described in a following section. Other modifications are sometimes necessary when the surface is covered by senesced vegetation that functions as an insulator of the surface.

In U.S. applications of METRIC, general approximate values of G/R_n=0.5 have been assigned for water and snow during the energy balance, representing values near midday. Snow is distinguished according to T_s<277 K, NDVI<0 and high surface albedo, and water is distinguished as NDVI<0 and low albedo. The G/R_n=0.5 for water should be refined according to the depth and turbidity of water bodies and time of season (Tasumi 2005; Allen and Tasumi 2005). G/R_n will be less than 0.5 for turbid or shallow water bodies due to the absorption of short-wave radiation near the water surface for turbid water and the reflection of solar radiation from and warming by the bottom for shallow systems. For 24 h periods, G/R_n will be somewhat less than the instantaneous value for water, but not necessarily zero (Allen et al. 2001). The G/R_n ratio for snow for 24 h periods is assumed to be nearly zero or somewhat positive during snowmelt.

Sensible Heat Flux

METRIC differs from previous applications of SEBAL principally in how the "H function" is calibrated for each specific satellite image. In both METRIC and SEBAL, H (W m^{-2}) is estimated from an aerodynamic function

$$H = \rho_{\mathrm{air}} C_p \frac{dT}{r_{\mathrm{ah}}} \tag{28}$$

where ρ_{air}=air density (kg m^{-3}); C_p=specific heat of air at constant pressure (J kg^{-1} K^{-1}); and r_{ah}=aerodynamic resistance (s m^{-1}) between two near surface heights, z_1 and z_2 (generally 0.1 and 2 m) computed as a function of estimated aerodynamic roughness of the particular pixel. In METRIC, the r_{ah} calculation uses wind speed extrapolated from some blending height above the ground surface (typically 100 to 200 m) and an iterative stability correction scheme based on the Monin–Obhukov functions (Allen et al. 1996). The dT parameter (K) represents the near-surface temperature difference between z_1 and z_2. dT is used in Eq. (28) because of the difficulty in estimating surface temperature (T_s) accurately from satellite due to uncertainty in atmospheric attenuation or contamination and radiometric calibration of the sensor. In addition, T_s, as measured by satellite (i.e., radiometric or kinetic temperature) can deviate from the "aerodynamic" temperature that drives the heat transfer process by several degrees (Kustas et al. 1994; Norman et al. 1995; Qualls and Brutsaert 1996). The temperature gradient dT is designed to "float" above the surface, beyond the height for sensible heat roughness (z_{oh}) and zero plane displacement, and can be approximated as a relatively simple linear function of T_s as pioneered by Bastiaanssen (1995)

$$dT = a + bT_{s\ \mathrm{datum}} \tag{29}$$

where a and b=empirically determined constants for a given satellite image, and $T_{s\mathrm{datum}}$=surface temperature adjusted to a common elevation data for each image pixel using a digital elevation model and customized lapse rate. Bastiaanssen (1995) provided empirical evidence for using the linear relation between dT and T_s. Theoretically, assuming some essentially constant temperature at a blending height well above the surface, for example at 100–200 m, where temperature is nearly independent of H, and with all instability effects incorporated into r_{ah}, Eq. (28) suggests that dT and thus, T_s, will be largely proportional to H for a fixed aerodynamic condition. Therefore, one can anticipate a segment of the temperature profile, represented by dT, to be proportional to both H and to T_s. The application of Eq. (29) appears to extend well across a range of surface roughnesses, because as roughness increases and r_{ah} decreases, dT, for the same value of H, decreases due to a more efficient transfer of H, and T_s reduces for the same reason. The determination of a and b is described in a following section. The use of dT indexed to T_s that does not rely on absolute values for T_s substantially reduces error in the calculation of H. This approach constitutes one of the pioneering components of the SEBAL model developed by Bastiaanssen (1995). The use of $T_{s\mathrm{datum}}$ in Eq. (29) corrects for cooling impacts on T_s due to increasing elevation within an image that are not related to dT and sensible heat flux.

Aerodynamic Transport

The value for r_{ah} is strongly influenced by the buoyancy within the boundary layer driven by the rate of sensible heat flux. Be-

cause both r_{ah} and H are unknown at each pixel, an iterative solution is required. During the first iteration, r_{ah} is computed assuming neutral stability

$$r_{ah} = \frac{\ln(z_2/z_1)}{u_* k} \tag{30}$$

where z_1 and z_2=heights above the zero-plane displacement of the vegetation where the endpoints of dT are defined; u_*=friction velocity (m s^{-1}), and k=von Karman's constant (0.41). Friction velocity u_* is computed during the first iteration using the logarithmic wind law for neutral atmospheric conditions

$$u_* = \frac{k u_{200}}{\ln(200/z_{om})} \tag{31}$$

where u_{200}=wind speed (m s^{-1}) at a blending height assumed to be 200 m, and z_{om}=momentum roughness length (m). z_{om} is a measure of the form drag and skin friction for the layer of air that interacts with the surface. u_* is computed for each pixel inside the process model using a specific roughness length for each pixel, but with u_{200} assumed to be constant over all pixels of the image since it is defined as occurring at a "blending height" unaffected by surface features. Eqs. (30) and (31) support the use of a temperature gradient defined between two heights that are both above the surface. This allows one to estimate r_{ah} without having to estimate a second aerodynamic roughness for sensible heat transfer (z_{oh}), since height z_1 is defined to be at an elevation above z_{oh}. This is an advantage because z_{oh} can be difficult to estimate for sparse vegetation.

The wind speed at an assumed blending height (200 m) above the weather station, u_{200}, is calculated as

$$u_{200} = \frac{u_w \ln(200/z_{omw})}{\ln(z_x/z_{omw})} \tag{32}$$

where u_w=wind speed measured at a weather station at z_x height above the surface and z_{omw}=the roughness length for the weather station surface, similar to Allen and Wright (1997). All units for z are the same. The value for u_{200} is assumed constant for the satellite image. This assumption allows for the use of a constant relation between dT and T_s.

Tasumi et al. (2005b) showed ET as calculated by METRIC to be relatively insensitive to the value for z_{om}. In METRIC, the momentum roughness length (z_{om}) is estimated for each pixel according to land use type or amount of vegetation. General land use type is used where the variation in z_{om} as a function of vegetation amount is not well established. General values are given in Brutsaert (1982) and Allen et al. (1996). In agricultural areas, z_{om} and, in turn, crop height is generally proportional to the LAI, and is therefore calculated as a function of LAI for "short" agricultural crops (less than about 1 m in height) using a relationship from Tasumi (2003)

$$z_{om} = 0.018 \text{ LAI} \tag{33}$$

where z_{om} has units of m and LAI is dimensionless. A minimum value for z_{om}=0.005 m represents roughness typical of bare agricultural soils. Eq. (33) tends to underestimate z_{om} for corn which is typically 2 to 3 m in height (Tasumi 2003), and a different function would be required for vines and trees. Because of the difficulties in estimating z_{om} from a general function of LAI for all vegetation types within an image, Bastiaanssen (2000) suggested customizing a function for z_{om} based on NDVI that is developed for each satellite image

$$z_{om} = \exp[(a_1 \text{NDVI}) + b_1] \tag{34a}$$

or, as modified by Allen (2002)

$$z_{om} = \exp[(a_1 \text{NDVI}/\alpha) + b_1] \tag{34b}$$

where a_1 and b_1=regression constants derived from a plot of $\ln(z_{om})$ versus NDVI or $\ln(z_{om})$ versus NDVI/α for two or more conditions in the image representing specific vegetation types. Eqs. (34*a*) and (34*b*) must be fitted to local vegetation and conditions. Generally α is lower for taller vegetation such as trees due to shading. Therefore, the use of albedo helps to distinguish between tall and short vegetation types that may have similar NDVI, but different albedo. Variations on Eqs. (34*a*) and (34*b*) can be explored by the user to improve the predictive accuracy, including use of other parameters.

The effects of mountainous terrain and elevation on wind speed are complicated and difficult to quantify (Oke 1987). In METRIC, z_{om} for image pixels in mountains is adjusted on a rudimentary basis to attempt to account for effects of general terrain roughness on momentum and heat transfer. An empirical adjustment is made by multiplying z_{om}, as calculated using Eqs. (33) and (34*a*) and (34*b*) or from general land classification, by a function determined locally in Idaho using slope as computed from a digital elevation model

$$z_{om\_mtn} = z_{om}\left(1 + \frac{(180/\pi)s - 5}{20}\right) \tag{35}$$

To further adjust the heat transfer equation for mountainous terrain, u_{200} at mountainous image pixels is multiplied by a wind speed weighting coefficient (ϖ) before computing u_* and r_{ah}. ϖ is calculated as

$$\varpi = 1 + 0.1\left(\frac{\text{Elevation} - \text{Elevation}_{\text{station}}}{1000}\right) \tag{36}$$

where Elevation=elevation of the pixel (m), and $\text{Elevation}_{\text{station}}$ =elevation where the wind speed is measured. Equations (35) and (36) were developed during METRIC applications in mountainous regions of southern Idaho (Tasumi 2003).

Air density in the aerodynamic equation is calculated using standard equations for mean atmospheric pressure and the universal gas law and simplifying for the effect of vapor pressure (virtual temperature is estimated as 1.01 T_s) as done by Allen et al. (1998)

$$\rho_{air} = \frac{1000P}{1.01(T_s - dT)R} \tag{37}$$

where ρ_{air}=air density (kg m^{-3})); P=mean atmospheric pressure for the pixel elevation (kPa); R=specific gas constant (287 J kg^{-1} K^{-1}); and $T_s - dT$=surrogate (K) for near-surface air temperature at the pixel.

Iterative Solution for r_{ah}

During subsequent iterations, a corrected value for u_* is computed as

$$u_* = \frac{u_{200} k}{\ln(200/z_{0\ \text{m}}) - \Psi_{m(200\ \text{m})}} \tag{38}$$

where $\psi_{m(200\ \text{m})}$=stability correction for momentum transport at 200 m [Eqs. (41) and (44)]. A corrected value for r_{ah} is computed for each iteration as

$$r_{ah} = \frac{\ln(z_2/z_1) - \Psi_{h(z_2)} + \Psi_{h(z_1)}}{u_* \times k} \quad (39)$$

where $\psi_{h(z2)}$ and $\psi_{h(z1)}$=stability corrections for heat transport at z_2 and z_1 heights [Eqs. (42) and (45)] that are updated each iteration.

Stability Correction Functions

The Monin–Obukhov length (L) defines the stability conditions of the atmosphere in the iterative process. L is the height at which forces of buoyancy (or stability) and mechanical mixing are equal, and is calculated as a function of heat and momentum fluxes

$$L = -\frac{\rho_{air} c_p u_*^3 T_s}{kgH} \quad (40)$$

where g=gravitational acceleration (=9.807 m s^{-2}) and units for terms cancel to m for L. Values of the integrated stability corrections for momentum and heat transport (ψ_m and ψ_h) are computed using formulations by Paulson (1970) and Webb (1970), depending on the sign of L. When $L<0$, the lower atmospheric boundary layer is unstable and when $L>0$, the boundary layer is stable. For $L<0$

$$\Psi_{m(200\ m)} = 2\ln\left(\frac{1+x_{(200\ m)}}{2}\right) + \ln\left(\frac{1+x_{(200\ m)}^2}{2}\right) - 2\arctan(x_{(200\ m)}) + 0.5\pi \quad (41)$$

$$\Psi_{h(2\ m)} = 2\ln\left(\frac{1+x_{(2\ m)}^2}{2}\right) \quad (42a)$$

$$\Psi_{h(0,1\ m)} = 2\ln\left(\frac{1+x_{(0.1\ m)}^2}{2}\right) \quad (42b)$$

where

$$x_{(200\ m)} = \left(1 - 16\frac{200}{L}\right)^{0.25} \quad (43a)$$

$$x_{(2\ m)} = \left(1 - 16\frac{2}{L}\right)^{0.25} \quad (43b)$$

$$x_{(0.1\ m)} = \left(1 - 16\frac{0.1}{L}\right)^{0.25} \quad (43c)$$

Values for $x_{(200\ m)}$, $x_{(2\ m)}$, and $x_{(0.1\ m)}$ have no meaning when $L \geq 0$ and their values are set to 1.0.

For $L>0$ (stable conditions)

$$\Psi_{m(200\ m)} = -5\left(\frac{2}{L}\right) \quad (44)$$

$$\Psi_{h(2\ m)} = -5\left(\frac{2}{L}\right) \quad (45a)$$

$$\Psi_{h(0.1\ m)} = -5\left(\frac{0.1}{L}\right) \quad (45b)$$

When $L=0$, the stability values are set to 0. Eq. (44) uses a value of 2 m rather than 200 m for z because it is assumed that under stable conditions, the height of the stable, inertial boundary layer is on the order of only a few meters. Using a larger value than 2 m for z can cause numerical instability in the model. For neutral conditions, $L=0$, $H=0$, and ψ_m and $\psi_h=0$.

Determination of Constants in the *dT* Function

In traditional applications of SEBAL (Bastiaanssen et al. 1998a, b), parameters a and b in Eq. (29) are computed by setting $dT=0$ for T_s equal to the surface temperature of a local water body (or in its absence, a well-vegetated field) and where SEBAL expects H to be zero. The dry end of the dT function is estimated by rearranging Eq. (28) for a selected "hot" pixel in the image where the soil is assumed to be dry enough so that $LE=0$

$$dT_{hot} = \frac{(R_n - G) r_{ah\ hot}}{\rho_{air\ hot} C_p} \quad (46)$$

where $r_{ah\ hot}=r_{ah}$ computed for the roughness and stability conditions of the hot pixel, and $\rho_{air\ hot}=\rho_{air}$ calculated at the hot pixel. The values for a and b in Eq. (29) are then estimated from these two pairs of dT and associated T_s.

In METRIC, a similar approach and assumptions are made for determining dT_{hot} for the hot pixel, although a daily surface soil water balance such as that of the FAO56 publication (Allen et al. 1998) is run for a bare soil condition to confirm that ET=0 or to supply a nonzero value for ET if there is residual evaporation (Suleiman and Ritchie 2003) from antecedent precipitation or other wetting event. Thus, in METRIC

$$H_{hot} = (R_n - G)_{hot} - LE_{hot} \quad (47)$$

from Eq. (1), where LE_{hot} is the latent residual evaporation at the hot pixel and R_n and G are values for the hot pixel.

At the "cold" pixel, we define the sensible heat flux in METRIC as

$$H_{cold} = (R_n - G)_{cold} - LE_{cold} \quad (48)$$

where LE_{cold}=estimated latent heat flux at the cold pixel. Experience shows that the coldest (and wettest) agricultural fields in a satellite image that are at full cover (LAI>4) have ET rates that are typically about 5% greater than the rate from the alfalfa reference crop ET_r (Tasumi 2003, Tasumi et al. 2005a). This occurs because, for a large population of fields, some fields will have a wet soil surface beneath a full vegetation canopy that will tend to increase the total ET rate to about 5% above that of the ET_r standard (Wright 1982). In addition, when viewing a large population of fields containing full cover alfalfa or other full cover crop, a specific subpopulation of fields will have somewhat wetter conditions due to recent irrigation and therefore a slightly higher ET and a slightly cooler temperature than the "mean" full cover condition represented by the standardized alfalfa reference. Also, the ET_r definition represents the mean evaporative condition for a 0.5 m tall alfalfa. Some of the alfalfa population (or other crops at full ground cover) will have ET rates above the mean. Hence, the value for LE_{cold} is based on a representative cold pixel selected from the satellite scene and is assumed to be $1.05 \times ET_r \times \lambda$, where λ is the latent heat of vaporization [from Eq. (53)].

Exceptions to the assumption that $ET_{cold}=1.05\ ET_r$ occur during nongrowing season periods and early in growing seasons where the amount of vegetation for the greenest and coolest pixels is less than that of the 0.5 m tall standardized alfalfa reference. In these cases, a ratio of $ET_{cold}/ET_r=f(NDVI)$ can be developed for the image, based on the judgement of the operator or based on local data. METRIC applications for agricultural crops in southern Idaho indicate that $ET_{cold}/ET_r \sim 1.25$ NDVI to 1.30 NDVI

during development periods, where NDVI is calculated without atmospheric correction (i.e., as a "top of atmosphere" value).
The near-surface temperature gradient over the cold pixel, dT_{cold}, is computed using the inverse of Eq. (28)

$$dT_{\text{cold}} = \frac{H_{\text{cold}} r_{\text{ah cold}}}{\rho_{\text{air cold}} C_p} \tag{49}$$

where $r_{\text{ah cold}} = r_{\text{ah}}$ computed for the roughness and stability conditions of the cold pixel, and $\rho_{\text{air cold}} = \rho_{\text{air}}$ calculated at the cold pixel.

The a and b coefficients are determined using the two pairs of values for dT and T_s where

$$a = \frac{dT_{\text{hot}} - dT_{\text{cold}}}{T_{s\ \text{datum hot}} - T_{s\ \text{datum cold}}} \tag{50}$$

and

$$b = [dT_{\text{hot}} - a]/T_{s\ \text{datum hot}} \tag{51}$$

where $T_{s\ \text{datum hot}}$ and $T_{s\ \text{datum cold}}$ = surface temperatures at the hot and cold pixels adjusted to a common elevation data for each image pixel using a digital elevation model and customized lapse rate.

In applications with MODIS, it is often difficult to find 1 km sized thermal pixels that contain homogenous vegetation that has sufficient ground cover to represent the "cold pixel" condition where ET $\sim 1.05\ \text{ET}_r$. Under these conditions, one can use METRIC applications based on and calibrated using Landsat to determine ET and $\text{ET}_r F$ for specific MODIS-scale pixels and to develop associated $\text{ET}_r F$ versus NDVI relationships for a target region that can in turn be used to determine the calibration for the coarse MODIS-based images (where pixels having $\text{ET}_r F = 1.05$ do not exist).

Calibration via Reference Evapotranspiration

METRIC uses the standardized ASCE Penman–Monteith equation for the alfalfa reference ET_r (ASCE-EWRI 2005) to calibrate the energy balance functions. ET_r is typically 20 to 30% greater than grass reference ET (ET_O). ET_r is used to approximate the ET of the cold pixel calibration condition because METRIC can be applied without crop classification, so that the specific crop type at any pixel is generally not known. Because the crop coefficient, K_c, typically peaks at 1.0 for many crops when using the alfalfa reference basis (Wright 1982; Jensen et al., 1990), the cold pixel can be nearly any agricultural crop with a complete ground cover and an LAI greater than approximately 4.0. The freedom from requiring crop classification constitutes a significant cost savings, as accurate crop classification from a satellite can be relatively costly.

Our confidence in the accuracy and dependability of the standardized ASCE Penman–Monteith equation for the calibration of the energy balance is strong. The equation has exhibited good sensitivity to hourly changes in weather, as demonstrated in Fig. 1, where measured and computed ET_r is compared hourly for 2 days near Kimberly, Idaho. The equation provides a robust approximation of the ET expected from extensive surfaces of full vegetation cover. Each satellite image is autocalibrated during the METRIC process using ET_r (calculated using hourly or shorter period weather data) via Eq. (48), where $LE_{\text{cold}} = 1.05\ \text{ET}_r \times \lambda$. The H_{cold} from Eq. (48) is in turn used in Eq. (49) to derive coefficients for Eqs. (50) and (51) for all pixels of the image.

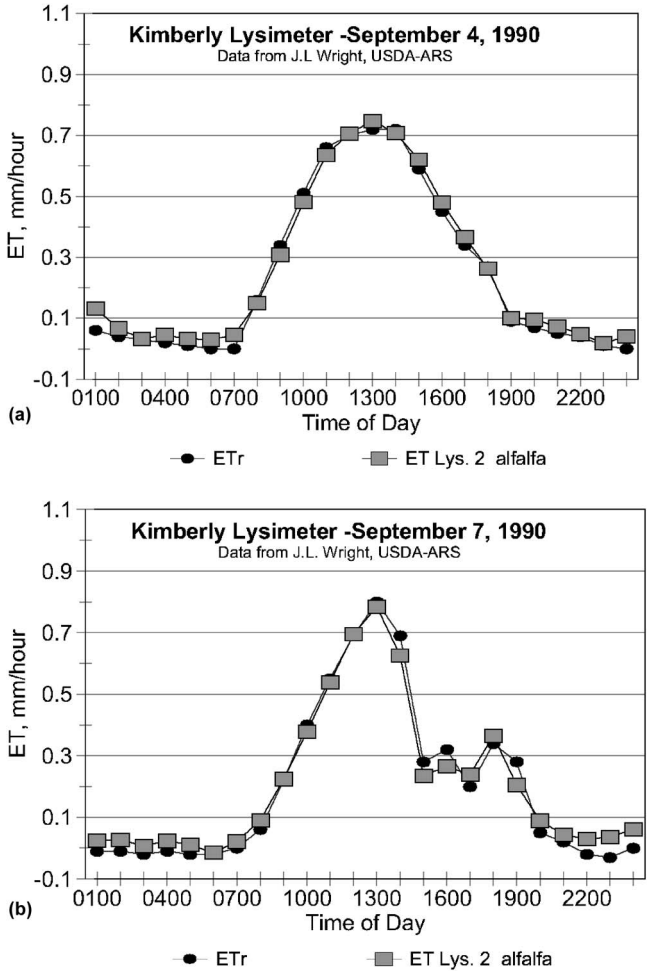

Fig. 1. Hourly calculated (ET_r) and measured (Lys. 2) alfalfa reference ET for two days: (a) clear day; (b) cloudy afternoon near Kimberly, Idaho [Lysimeter data from Wright (1982) USDA-ARS]

The calibration of the sensible heat process equations, and in essence the entire energy balance, to ET_r corrects the surface energy balance for lingering systematic computational biases associated with empirical functions used to estimate some components and uncertainties in other estimates as summarized by Allen et al. (2005), including:

- Atmospheric correction;
- Albedo calculation;
- Net radiation calculation;
- Surface temperature from the satellite thermal band;
- Air temperature gradient function used in sensible heat flux calculation;
- Aerodynamic resistance including stability functions;
- Soil heat flux function; and
- Wind speed field.

This list of biases essentially plagues all surface energy balance computations that utilize satellite imagery as the primary spatial information resource. Most polar orbiting satellites orbit about 700 km above the Earth's surface, yet the transport of vapor and sensible heat from land surfaces is strongly impacted by aerodynamic processes including wind speed, turbulence, and buoyancy, all of which are essentially invisible to satellites. In addition, the precise quantification of albedo, net radiation, and soil heat flux is uncertain and potentially biased. Therefore, even though the best efforts are made to estimate each of these parameters as accu-

rately and as unbiased as possible, some biases do occur and calibration to ET_r helps to compensate for this by introducing a bias correction into the calculation of H. The end result is that biases inherent to R_n, G, and subcomponents of H are essentially cancelled by the subtraction of a bias-canceling estimate for H. The result is an ET map with values ranging between near zero and near ET_r, for images with a range of bare or nearly bare soil and full vegetation cover.

Adjustment to Empirical Equations

METRIC utilizes a number of empirical equations to estimate values to support various components of the energy balance. These equations include those for leaf area index, aerodynamic roughness length, soil heat flux, and air temperature gradient. Users may be concerned about whether these component estimates or the METRIC calibration process may break down under specific circumstances. The empirical equations applied are, in principle, considered to be relatively robust in their transferability. The use of ET_r to calibrate each application corrects for much of the individual bias introduced into a component estimate. For example, Tasumi (2003) found less than a few percent error in METRIC ET when estimates for z_{om} were halved and doubled prior to METRIC calibration. The calibration process adjusted the calibration of the dT function to account for the decreased or increased bias in roughness and therefore estimates for H and ET were minimally impacted. In addition, the energy balance process is only slightly sensitive to roughness for areas having ET within 30% of ET_r because the total value for H is small. Also, the process is only slightly sensitive to roughness at low values for ET, since boundary layer buoyancy dominates the sensible heat exchange.

Several applications of METRIC have required a modification of the empirical functions for G. In an application to Imperial Valley, California, soil heat transfer into desert soils was reduced by crusts detached from the underlying soil. In this situation, desert soils had significantly higher surface temperature than bare agricultural soils due to the reduced G. Values for G estimated empirically were reduced in proportion to surface temperature above a threshold value.

In applications in southern Idaho, sparsely vegetated desert systems, although aerodynamically rough, have a characteristically high surface temperature. The combination of high z_{om} and high T_s causes an overestimation of H when using the same dT versus T_s function developed for agricultural regions of the satellite image. The overestimation of H has been largely overcome by adding an "excess resistance" term to r_{ah} to account for the sheltering effect of the desert canopy. The function for the excess resistance was empirically developed using eddy covariance and temperature gradient measurements made over the sagebrush environment and was expressed as a closed function of wind speed.

In applications along the Middle Rio Grande of New Mexico (described in Allen et al. 2007), two separate dT functions were developed and applied for each image. One dT function was applied to agricultural areas within the Rio Grande valley, which tends to be incised below the regional plain, and the other dT function was applied to areas outside the valley. The two functions were required due to substantially different surface temperatures exhibited for the "dry pixels." In some applications containing desert systems, the slope of the dT function in Eq. (29) is reduced when $T_{s\ \mathrm{datum}}$ exceeds the $T_{s\ \mathrm{datum\ hot}}$ hot of the hot pixel. These deviations from routine application of METRIC equations are examples of modifications to the empirical method that may be required to improve accuracy of estimates of ET from natural systems, and illustrate the value of specific knowledge of native systems, principles of aerodynamic transfer and boundary layer development, soil physics, and energy transfer limitations. Future study and additional sensitivity assessments of impacts of empirical estimates for various energy balance components are warranted.

Calculation of Evapotranspiration

ET at the instant of the satellite image is calculated for each pixel by dividing LE from Eq. (1) by latent heat of vaporization

$$\mathrm{ET_{inst}} = 3{,}600\frac{\mathrm{LE}}{\lambda\rho_w} \tag{52}$$

where ET_{inst}=instantaneous ET (mm h^{-1}); 3,600 converts from seconds to hours, ρ_w=density of water ($\sim$1,000 kg m^{-3}); and λ=latent heat of vaporization (J kg^{-1}) representing the heat absorbed when a kilogram of water evaporates and is computed as

$$\lambda = [2.501 - 0.00236(T_s - 273.15)] \times 10^6 \tag{53}$$

The reference ET fraction (ET_rF) is calculated as the ratio of the computed instantaneous ET (ET_{inst}) from each pixel to the reference ET (ET_r) computed from weather data

$$\mathrm{ET}_r F = \frac{\mathrm{ET_{inst}}}{\mathrm{ET}_r} \tag{54}$$

where ET_{inst} is from Eq. (52) (mm h^{-1}) and ET_r is for the standardized 0.5 m tall alfalfa reference at the time of the image. Generally only one or two weather stations are required to estimate ET_r for a Landsat image that measures 180×180 km, as discussed later. ET_rF is the same as the well-known crop coefficient, K_c, when used with an alfalfa reference basis, and is used to extrapolate ET from the image time to periods of 24 h or longer.

One should generally expect ET_rF values to range from 0 to about 1.0 (Wright 1982; Jensen et al. 1990). At a completely dry pixel, ET=0 and therefore ET_rF=0. A pixel in a well established field of alfalfa or corn can occasionally have an ET slightly greater than ET_r and therefore $ET_rF > 1$, perhaps up to 1.1 if it has been recently wetted by irrigation or precipitation. However, ET_r generally represents an upper bound on ET for large expanses of well-watered vegetation. Negative values for ET_rF can occur in METRIC due to systematic errors caused by various assumptions made earlier in the energy balance process and due to random error components so that error should oscillate about ET_rF=0 for completely dry pixels. In calculation of ET_rF in Eq. (54) each pixel retains a unique value for ET_{inst}, that is derived from a common value for ET_r, derived from the representative weather station data.

24-Hour *Evapotranspiration* (ET_{24})

Daily values of ET (ET_{24}) are generally more useful than the instantaneous ET that is derived from the satellite image. In the METRIC process, ET_{24} is estimated by assuming that the instantaneous ET_rF computed at image time is the same as the average ET_rF over the 24 h average. Fig. 2 shows a series of graphs of ET and ET_rF versus time for a sugar beet crop that demonstrates that ET_rF is relatively constant throughout a day. The August dates shown in the figure had full ground cover. Similar examples for grass are shown in Allen et al. (2007). Romero (2004) demon-

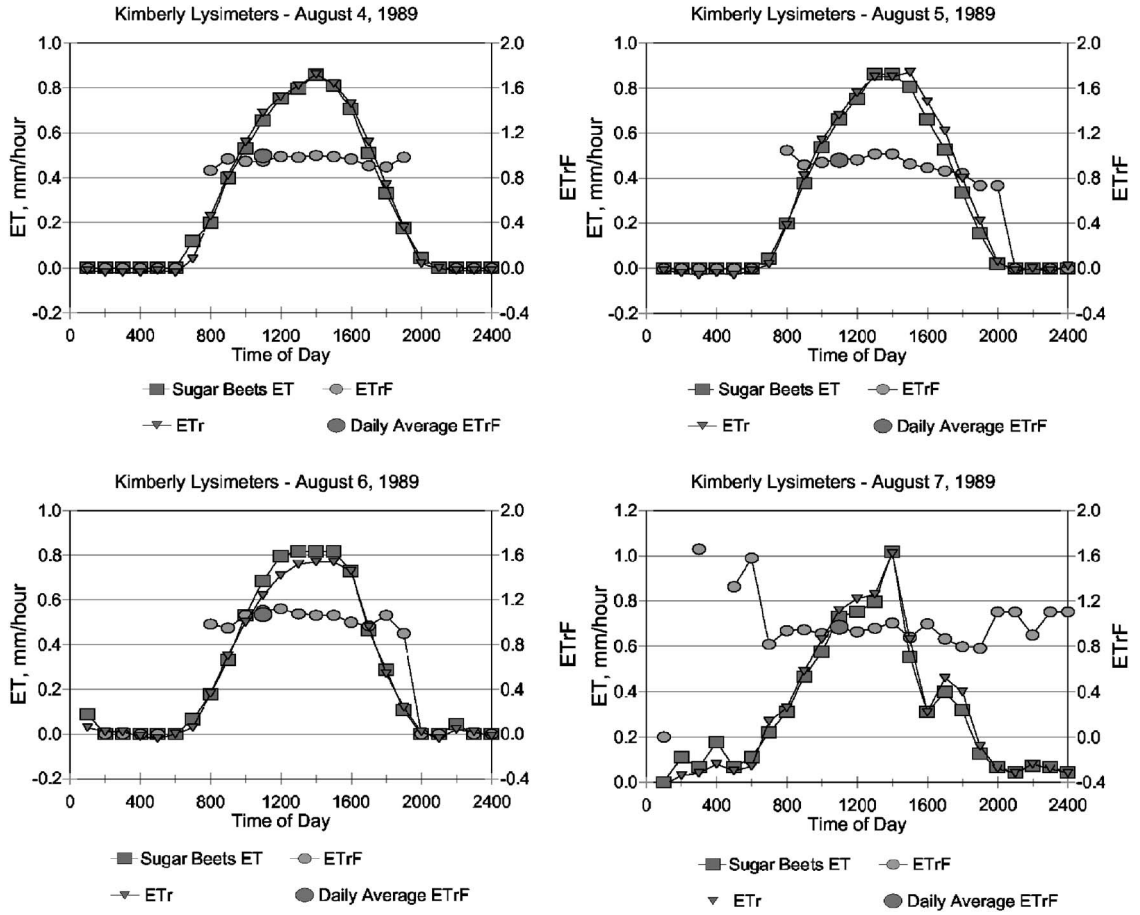

Fig. 2. Hourly ET and ET_rF for sugar beet crop versus time [based on lysimeter observations by Wright (1982), USDA-ARS, Kimberly, Idaho] for a series of four days in August (ET_rF for the 24 h period is the larger circle plotted at 11:00, which is satellite overpass time)

strated relative constancy of ET_rF during the day for crops of potatoes, corn, and beans based on lysimeter data from the USDA-ARS at Kimberly, Idaho (Wright 1982).

Fig. 3(a) shows lysimeter measurements of ET_rF at satellite overpass time versus ET_rF for the 24 h period on satellite image days, and Fig. 3(b) shows the same parameters, but for all measured days during the year. Agreement between instantaneous and 24 h average ET_rF is relatively good, indicating the advantage of using ET_r and the assumption of constant ET_rF during the day as a time-based transfer mechanism. ET_r tends to encapsulate advective effects of regional weather on ET.

The assumption of constant ET_rF during a day appears to be generally valid for agricultural crops that have been developed to maximize photosynthesis and thus stomatal conductance. ET_rF may decrease during the afternoon for some native vegetation under water short conditions, where plants endeavor to conserve soil water. Under these conditions, the 24 h ET_rF must be modeled as some fraction of instantaneous ET_rF. This requires local study and measurement to develop the needed functions.

Finally, the ET_{24} (mm/day) is computed for each image pixel as

$$ET_{24} = C_{rad}(ET_rF)(ET_{r\_24}) \tag{55}$$

where ET_rF is assumed equal to the ET_rF determined at the satellite overpass time; ET_{r-24}=cumulative 24 h ET_r for the day of the image; and C_{rad}=correction term used in sloping terrain to correct for variation in 24 h versus instantaneous energy availability. C_{rad} is calculated for each image and pixel as

$$C_{rad} = \frac{R_{so(inst)Horizontal}}{R_{so(inst)Pixel}} \cdot \frac{R_{so(24)Pixel}}{R_{so(24)Horizontal}} \tag{56}$$

where R_{so}=clear-sky solar radiation (W m^{-1}), the "(inst)" subscript denotes conditions at the satellite image time; "(24)" represents the 24 h total; the "Pixel" subscript denotes slope and aspect conditions at a specific pixel, and the "Horizontal" subscript denotes values calculated for a horizontal surface representing the conditions impacting ET_r at the weather station. For applications to horizontal areas, C_{rad}=1.0.

The 24 h R_{so} for horizontal surfaces and for sloping pixels is calculated as

$$R_{so(24)} = \int_0^{24} R_{so\_i} \tag{57}$$

where R_{so_i}=instantaneous clear-sky solar radiation at time i of the day, calculated by Eq. (3). In METRIC, ET_{r24} is calculated by summing hourly ET_r values over the day of the image.

There is some question regarding whether the dT function responds correctly in regions of a satellite image where wind and thus ET_r have different values. In the application of METRIC, a single dT function is generally developed for an entire image or for a subregion of an image where T_s exhibits a similar range. Investigations in Idaho (Trezza 2002; Tasumi 2003) have indicated that where wind speed is higher and thus ET is higher in a subregion relative to the region of dT calibration, values for T_s tend to run slightly lower. The lower T_s causes lower dT estimates

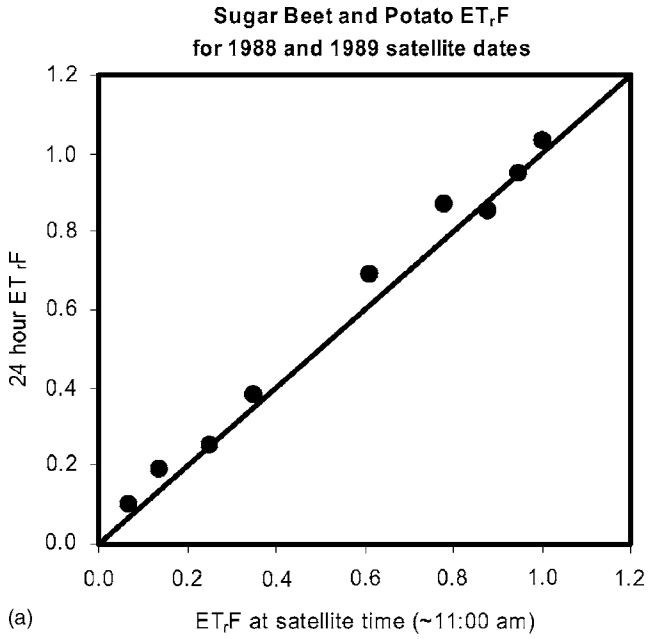

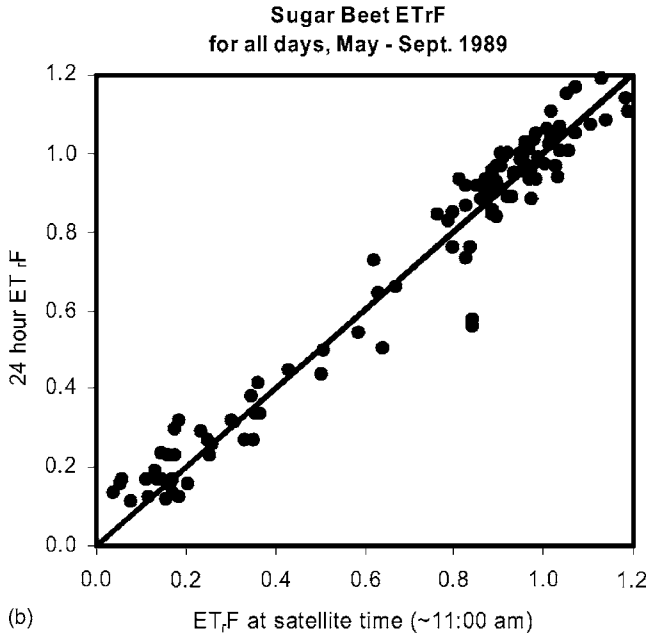

Fig. 3. ET_rF for the 24 h period versus ET_rF at satellite time for: (a) satellite image days processed in 1988 and 1989; (b) for all days measured by lysimeter for a sugar beet crop in 1989 [lysimeter data from Wright (1982) USDA-ARS]

that in turn produce higher ET. Therefore, even though wind speed and ET_r for the subregion deviate from that for the image subregion of calibration, the ET may be more accurately predicted using the general dT function [Eq. (29)] established for the image date when wind speed is held constant in space.

Following the determination of ET and ET_rF for a subregion having different ET_r and wind speed, however, it may be advantageous to apply an ET_r value specific to that sub area when interpolating to 24 h ET and for interpolating between satellite image dates. In other words, it appears possible to limit the number of weather stations used to define ET_r and average wind speed during dT calibration and energy balance computations, but then use additional stations when multiplying ET_rF by ET_r. When in doubt whether the derived dT function fits all regions of an image, the user should consider dividing the image into multiple regions and develop a unique METRIC application and calibration for each subimage area. Except in narrow mountain valleys, ET_r is relatively stable and often representative for areas of 50–100 km distance with relatively small changes. Thus, if the weather station is in the center of a Landsat image, then a single station may be appropriate to use in computing $ET_rF \times ET_r$. Local tests and comparisons should be made. Users need to recognize that what appear to be differences in ET_r between weather stations may actually be caused by faulty and biased weather measurements (Allen et al. 1998; ASCE-EWRI 2005). Future studies are needed to investigate the impact of variation in ET_r, the dT function, and wind speed on variation in actual ET within an image, given the same vegetation amounts.

A study of repeatability of METRIC application—by two independent operators using two different sets of weather stations and two different overlapping Landsat paths and satellite image dates (Tasumi et al. 2005b)—showed some variation in estimated ET caused by a combination of the differences between the two applications, including differences in reference ET_r. However, repeatability and consistency in monthly and seasonal ET estimates was relatively good.

Seasonal Evapotranspiration ($ET_{seasonal}$)

Monthly and seasonal evapotranspiration "maps" are often desired for quantifying total water consumption from agriculture. These maps can be derived from a series of ET_rF images by interpolating ET_rF between processed images and multiplying, on a daily basis, by the ET_r for each day. The interpolation of ET_rF between image dates is not unlike the construction of a seasonal K_c curve, where interpolation is done between discrete values for K_c.

The METRIC approach assumes that the ET for the entire area of interest changes in proportion to change in ET_r at the weather station. This is a generally valid assumption and is similar to the assumptions used in the conventional application of $K_c \times ET_r$. This approach is effective in estimating ET for both clear and cloudy days in between the clear-sky satellite image dates (Tasumi et al. 2005a). The assumption is further supported by the use of ET_r from the same weather location as is used to derive ET_rF at image time, so that any biases caused by differing weather conditions in some part of an image will be predominately cancelled by using the same ET_rF for both instantaneous and 24 h period as well as for days between image dates. ET_r is computed at a specific weather station location and therefore does not represent the actual condition at each pixel. However, because ET_r is used only as an index of the relative change in weather, specific information at each pixel is retained through the ET_rF.

The cumulative ET for any period, for example, month, season, or year, is calculated as

$$ET_{period} = \sum_{i=m}^{n} [(ET_rF_i)(ET_{r24i})] \quad (58)$$

where ET_{period}=cumulative ET for a period beginning on day m and ending on day n, ET_rF_i=interpolated ET_rF for day i; and ET_{r24i}=24 h ET_r for day i. Units for ET_{period} will be in mm when ET_{r24} is in mm day^{-1}. The interpolation between values for ET_rF can be made using linear interpolation or using a curvilinear in-

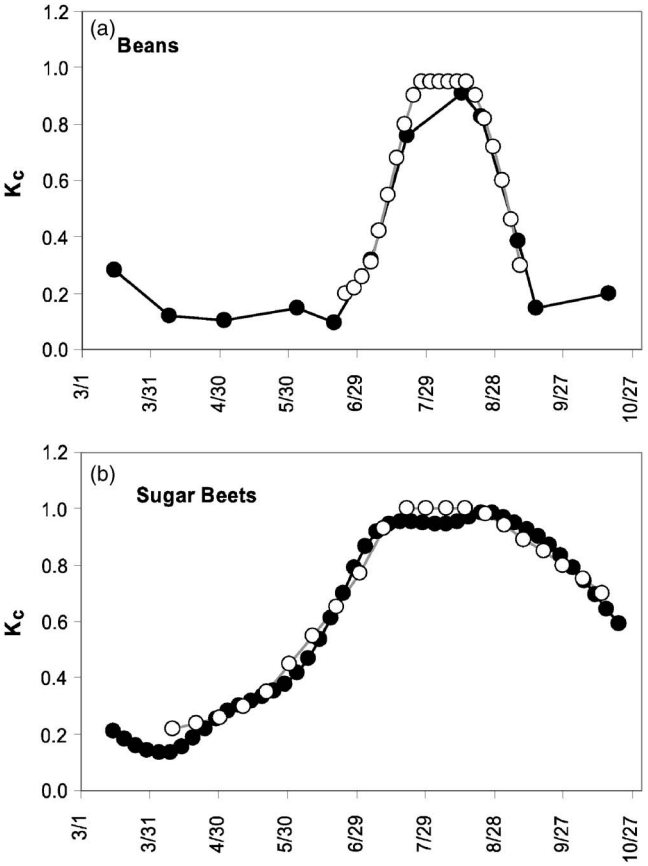

Fig. 4. ET_rF from METRIC for: (a) dry bean crop in southern Idaho in 2000 (solid symbols) compared to a K_c curve [published by the USBR AgriMet (2000) (open circles) (adapted from Tasumi et al. 2005a,b]; (b) sugar beet crop where a cubic spline has been used to interpolate between satellite image dates

terpolation function, for example, a spline function, to better fit the typical curvilinearity of crop coefficients during a growing season (Wright 1982). Generally one satellite image per month is sufficient to construct an accurate ET_rF curve for purposes of estimating seasonal ET. During periods of rapid vegetation change, a more frequent image interval may be desirable, as illustrated in Fig. 4(a), where the lack of satellite image in mid-July caused an underestimation of the ET_rF (i.e., K_c) curve for dry beans near the beginning of the midseason, when ET_rF was interpolated linearly between satellite dates. Spline interpolation would have moved the interpolated value closer to the USBR Agrimet (2000) curve, as shown for the example of sugar beets in Fig. 4(b).

If a specific pixel must be masked out of an image because of cloud cover, then a subsequent image date must be used during the interpolation and the estimated ET_rF or the K_c curve will have reduced accuracy. In actuality, ET_rF (i.e., K_c) varies substantially from day to day as shown in Fig. 4 of Allen et al. (2007), primarily due to the variability in weather data and surface wetness. Therefore, the continuous K_c (i.e., ET_rF) curve, whether constructed from a published curve or table, or estimated from METRIC, is only an approximation of the actual K_c (i.e., ET_rF) on any specific day.

Average ET_rF over a Period

An average ET_rF for the period can be calculated as

$$ET_rF_{\text{period}} = \frac{\sum_{i=m}^{n} [(ET_rF_i)(ET_{r24i})]}{\sum_{i=m}^{n} ET_{r24i}} \quad (59)$$

ET_rF versus EF

METRIC and its original basis SEBAL differ somewhat in the extrapolation of instantaneous ET to the 24 h period. In traditional applications of SEBAL, the evaporative fraction (EF) is used rather than ET_rF. EF is defined as the ratio of ET to available energy, R_n-G, and EF is assumed to be the same at both the observation time and for the 24 h period. The assumption of constant EF during the day can underpredict 24 h ET in arid climates where afternoon advection or increased afternoon wind speed may increase ET in proportion to R_n-G. In METRIC, the assumption of constant ET_rF during the day is better able to capture any impacts of advection and changing wind and humidity conditions during the day, as these are expressed in the ET_r calculation (which is made hourly and summed daily). Trezza (2002) and Romero (2004) demonstrated the general validity of constant ET_rF during the day using lysimeter data from Kimberly, Idaho (Wright 1982).

Summary and Conclusions

METRIC is a satellite-based image-processing tool for calculating ET as a residual of the energy balance at the Earth's surface. METRIC has, as its foundation, principles and techniques used by the important model SEBAL; an energy balance model developed in The Netherlands and applied worldwide by Bastiaanssen and his associates (1995, 1998a,b, 2000, 2005). In particular, METRIC uses the SEBAL technique for estimating the near-surface temperature gradient, dT, as an indexed function of radiometric surface temperature, thereby eliminating the need for absolutely accurate aerodynamic surface temperatures and air-temperature measurements for estimating sensible heat flux at the surface. METRIC utilizes the internal calibration of the satellite-based energy balance at two extreme conditions (dry and wet) using locally available weather data. The autocalibration is done for each image using an alfalfa-based reference ET (ET_r) computed from hourly weather data. The internal calibration and the use of the indexed temperature gradient eliminate the need for atmospheric correction of T_s and reflectance (albedo) measurements using radiative transfer models. The internal calibration also reduces impacts of biases in estimating the aerodynamic stability correction and surface roughness.

METRIC and SEBAL represent a maturing technology for deriving a satellite-driven surface energy balance for estimating ET from the Earth's surface, and have the potential to become widely adopted by water resources communities. METRIC is designed to produce high quality and accurate maps of ET for focused regions smaller than a few hundred kilometers in scale and at high resolution. Thus, use of reference ET for calibration and for extrapolating from instantaneous to 24 h ET helps account for regional advection effects on ET and improves congruency with the traditional reference ET $\times K_c$ approach. Requirements for applying

METRIC are trained experts with a good background in energy balance, radiation physics and an adequate knowledge of vegetation characteristics, as well as high quality hourly (or shorter) weather data.

The requirements for trained experts to possess a strong physics background and high quality weather data create a distinct disadvantage of METRIC in that highly specialized personnel are required to operate the model for credibility. It is evident that METRIC is highly reliant on the operator's ability to select appropriate cold and hot pixels. It is currently not a hands-off model. Future work will include use of statistical relationships within images to help automate the identification and selection of the cold and hot pixels and thus general calibration. The application of energy balance to a wide mixture of agricultural crops and other vegetation is complex enough that there are still some areas of considerable empiricism and therefore potential for local refinement.

Acknowledgments

The writers acknowledge the long-term lysimeter data collection by Dr. James L. Wright, USDA-ARS, Kimberly, Idaho, that provided the means for comparing ET measurements with ET estimated by METRIC, and for confirming the relative constancy of $ET_r F$ during daylight hours. They also acknowledge the positive feedback on model focus by Tony Morse and Bill Kramber of the Idaho Department of Water Resources, and the initial training by and very informative and helpful discussions with Dr. Wim Bastiaanssen of WaterWatch, The Netherlands, that significantly boosted the development and characteristics of METRIC. Funding for the various applications and development came from NASA, Raytheon, USDA-CSREES, Idaho Department of Water Resources, U.S. Bureau of Reclamation, Metropolitan Water District of Southern California, U.S. Dept. of Justice, Keller-Bliesner Engineering, Idaho Agricultural Experiment Station, and Idaho Engineering Experiment Station. The writers acknowledge the very helpful comments and suggestions by reviewers to improve the clarity of this manuscript.

References

Allen, R. G. (1996). "Assessing integrity of weather data for use in reference evapotranspiration estimation." *J. Irrig. Drain. Eng.*, 122(2), 97–106.

Allen, R. G. (2002). "Evapotranspiration for southwest Florida from satellite-based energy balance." *Rep. Prepared for Tampa Bay Water*, Tampa Bay, Fla.

Allen, R. G., et al. (1996). Chap. 4 "Evaporation and transpiration." Wootton et al., eds., *ASCE handbook of hydrology*, ASCE, Reston, Va., 125–252.

Allen, R. G., Bastiaanssen, W., Tasumi, M., and Morse, A. (2001). "Evapotranspiration on the watershed scale using the SEBAL model and Landsat images." *Proc., 2001 ASAE Annual Int. Meeting*, ASAE, St. Joseph, Mich., Paper No. 01-2224.

Allen, R. G., Hartogensis, O., and de Bruin, H. (2000). "Long-wave radiation over alfalfa during the RAPID field campaign in southern Idaho." *Research Report*, Kimberly, Univ. of Idaho, Id.

Allen, R. G., Pereira, L. S., Raes, D., and Smith, M. (1998). "Crop evapotranspiration: Guidelines for computing crop water requirements." *United Nations FAO, Irrigation and Drainage*, N.Y., Paper No. 56. ⟨http://www.fao.org/docrep/X0490E/X0490E00.htm⟩ (February 5, 2007).

Allen, R. G., and Tasumi, M. (2005). "Evaporation from American Falls Reservoir in Idaho via a combination of Bowen ratio and eddy covariance." *Proc., EWRI World Water and Environmental Resources Congress 2005: Impacts of Global Climate Change*. EWRI, Reston, Va.

Allen, R. G., Tasumi, M., and Trezza, R. (2005). "Benefits from tying satellite-based energy balance to ground-based reference evapotranspiration." *AIP Conf. Proc.*, 852 127–137.

Allen, R. G., Tasumi, M., and Trezza, R. (2007). "Satellite-based energy balance for mapping evapotranspiration with internalized calibration (METRIC)—Applications." *J. Irrig. Drain. Eng.*, 133(4), 395–406.

Allen, R. G., and Wright, J. L. (1997). "Translating wind measurements from weather stations to agricultural crops." *J. Hydrol. Eng.*, 2(1), 26–35.

Anderson, M. C., et al. (2004). "A multiscale remote sensing model for disaggregating regional fluxes to micrometeorological scales." *J Hydrometeorol.*, 5, 343–363.

ASCE–EWRI. (2005). "The ASCE standardized reference evapotranspiration equation." *ASCE–EWRI Standardization of Reference Evapotranspiration Task Committe Rep.*, ASCE Reston, Va.

Bastiaanssen, W. G. M. (1995). "Regionalization of surface flux densities and moisture indicators in composite terrain: A remote sensing approach under clear skies in Mediterranean climates." Ph.D. Dissertation, CIP Data Koninklijke Bibliotheek, Den Haag, The Netherlands.

Bastiaanssen, W. G. M. (1998a). "Remote sensing in water resources management: The state of the art." International Water Management Institute, Colombo, Sri Lanka.

Bastiaanssen, W. G. M. (1998b). "The surface energy balance algorithm for land (SEBAL). 2: Validation." *J. Hydrol.*, 212–213, 213–229.

Bastiaanssen, W. G. M. et al. (2005). "SEBAL model with remotely sensed data to improve water-resources management under actual field conditions." *J. Irrig. Drain. Eng.*, 131(1), 85–93.

Bastiaanssen, W. G. M. (2000). "SEBAL-based sensible and latent heat fluxes in the irrigated Gediz Basin, Turkey." *J. Hydrol.*, 229, 87–100.

Bastiaanssen, W. G. M., Menenti, M., Feddes, R. A., and Holtslag, A. A. M. (1998). "A remote sensing surface energy balance algorithm for land (SEBAL): 1. Formulation." *J. Hydrol.*, 212–213, 198–212.

Berk, A. et al. (1999). "MODTRAN4 radiative transfer modeling for atmospheric correction." *Proc. SPIE*, 3756(1), 348–353.

Betts, A. K., Chen, F., Mitchell, K. E., and Janjic, Z. I. (1997). "Assessment of the land surface and boundary layer models in two operational versions of the NCEP Eta model using FIFE data." *Mon. Weather Rev.*, 125, 2896–2916.

Brutsaert, W. (1982). *Evaporation into the atmosphere*, Reidel, Dordrecht, The Netherlands.

Chander, G., and Markham, B. (2003). "Revised Landsat-5 TM radiometric calibration procedures and postcalibration dynamic ranges." *IEEE Trans. Geosci. Remote Sens.*, 41(11), 2674–2677.

Duffie, J. A., and Beckman, W. A. (1980). *Solar engineering of thermal process*, 1st Ed., Wiley, N.Y.

Duffie, J. A., and Beckman, W. A. (1991). *Solar engineering of thermal process*, 2nd Ed., Wiley, N.Y.

Garrison, J. D., and Adler, G. P. (1990). "Estimation of precipitable water over the United States for application to the division of solar radiation into its direct and diffuse components." *Sol. Energy*, 44(4), 225–241.

Granger, R. J. (1989). "Evaporation from natural nonsaturated surfaces." *J. Hydrol.*, 111, 21–29.

Granger, R. J. (2000). "Satellite-derived estimates of evapotranspiration in the Gediz Basin." *J. Hydrol.*, 229(1–2), 70–76.

Huete, A. R. (1988). "A soil adjusted vegetation index (SAVI)." *Remote Sens. Environ.*, 25, 295–309.

Jensen, M. E., Burman, R. D., and Allen, R. G., eds. (1990). "Evapotranspiration and irrigation water requirements." *ASCE Manuals and Reports on Engineering Practice No. 70*, ASCE, Reston, Va.

Kustas, W. P., et al. (1994). "Surface energy balance estimates at local and regional scales using optical remote sensing from an aircraft platform and atmospheric data collected over semiarid rangelands." *Water Resour. Res.*, 30(5), 1241–1259.

LPSO. (2004). *Landsat 7 science data users handbook*, Landsat Project Science Office, NASA Goddard Space Flight Center, Greenbelt, Md., ⟨http://ltpwww.gsfc.nasa.gov/IAS/handbook/handbook_toc.html⟩ (Feb. 5, 2007).

Majumdar, N. C., Mathur, B. L., and Kaushik, S. B. (1972). "Prediction of direct solar radiation for low atmospheric turbidity," *Sol. Energy*, 13, 383–394.

Markham, B. L., and Barker, J. L. (1986). "Landsat MSS and TM post-calibration dynamic ranges, exoatmospheric reflectances and at-satellite temperatures." *EOSAT Landsat Technical Notes 1:3-8*, Earth Observation Satellite Company, Lanham, Md.

MODIS UCSB Emissivity Library. (2004). "MODIS University of California Santa Barbara." ⟨http://www.icess.ucsb.edu/modis/EMIS/html/em.html⟩ (Feb. 5, 2007).

Norman, J. M., Kustas, W. P., and Humes, K. S. (1995). "Source approach for estimating soil and vegetation energy fluxes in observations of directional radiometric surface temperature." *Agric. Forest Meteorol.*, 77, 263–293.

Oke, T. R. (1987), *Boundary layer climates*, 2nd Ed., Methuen, London.

Paulson, C. A. (1970). "The mathematical representation of wind speed and temperature profiles in the unstable atmospheric surface layer." *J. Appl. Meteorol.*, 9, 857–861.

Qualls, R., and Brutsaert, W. (1996). "Effect of vegetation density on the parameterization of scalar roughness to estimate spatially distributed sensible heat fluxes." *Water Resour. Res.*, 32(3), 645–652.

Romero, M. G. (2004). "Daily evapotranspiration estimation by means of evaporative fraction and reference ET fraction." Ph.D. dissertation, Utah State Univ., Logan, Utah.

Suleiman, A. A., and Ritchie, J. T. (2003). "Modeling soil water redistribution during second-stage evaporation." *Soil Sci. Soc. Am. J.*, 67, 377–386.

Tasumi, M. (2003). "Progress in operational estimation of regional evapotranspiration using satellite imagery." Ph.D. dissertation, Univ. of Idaho, Moscow, Id.

Tasumi, M. (2005). "A review of evaporation research on Japanese lakes." *Proc. ASCE/EWRI World Water and Environmental Resources Congress*, ASCE, Reston, Va.

Tasumi, M., Allen, R. G., and Trezza, R. (2007). "Estimation of at-surface reflectance and albedo from satellite for routine, operational calculation of land surface energy balance." *J. Hydrol. Eng.*.

Tasumi, M., Allen, R. G., Trezza, R., and Wright, J. L. (2005a). "Satellite-based energy balance to assess within-population variance of crop coefficient curves." *J. Irrig. Drain. Eng.*, 131(1), 94–109.

Tasumi, M., Trezza, R., Allen, R. G., and Wright, J. L. (2005b). "Operational aspects of satellite-based energy balance models for irrigated crops in the semi-arid U.S." *Irrig. Drain. Syst.*, 19, 355–376.

Trezza, R. (2002). "Evapotranspiration using a satellite-based surface energy balance with standardized ground control." Ph.D. dissertation, Utah State Univ., Logan, Utah.

USBR. (2000). AgriMet: Pacific Northwest Cooperative Agricultural Weather Network. ⟨www.usbr.gov/pn/agrimet⟩ (June 9, 2007).

Van Dam, R. L., Borchers, B., and Hendrickx, J. M. H. (2005). "Strength of landmine signatures under different soil conditions: implications for sensor fusion." *Int. J. Syst. Sci.*, 36, 573–588.

Webb, E. K. (1970). "Profile relationships: the log-linear range, and extension to strong stability." *Q. J. R. Meteorol. Soc.*, 96, 67–90.

Wigmosta, M. S., Vail, L., and Lettenmaier, D. P. (1994). "A distributed hydrology-vegetation model for complex terrain." *Water Resour. Res.*, 30, 1665–1679.

Wright, J. L. (1982). "New evapotranspiration crop coefficients." *J. Irrig. and Drain. Div.*, 108, 57–74.

Wukelic, G. E., Gibbons, D. E., Martucci, L. M., and Foote, H. P. (1989). "Radiometric calibration of Landsat thematic mapper thermal band." *Remote Sens. Environ.*, 28, 339–347.